

# One-Step Two-Dimensional Microfluidics-Based Synthesis of Three-Dimensional Particles

Navid Hakimi, Scott S. H. Tsai, Chil-Hung Cheng, and Dae Kun Hwang\*

Manufactured microparticles have numerous emerging application areas, namely, in drug delivery,<sup>[1]</sup> tissue engineering,<sup>[2]</sup> particle-assembly,<sup>[3]</sup> and microelectromechanical systems (MEMS)<sup>[4]</sup> among others. One of the most important properties of microparticles in their applications is their shape.<sup>[5]</sup> For example, in microparticle-based drug delivery, the shape of the delivery vehicle is an important parameter that determines the diffusion and penetration properties of the drug.<sup>[6]</sup> In therapeutics and diagnostics applications, a biological event can be enhanced by simply changing the particle shape.<sup>[7]</sup> In microfluidic cell sorting by electromagnetic<sup>[8]</sup> or acoustic forcing,<sup>[9]</sup> the living cells being sorted have three-dimensional (3D) features that influence the cell trajectory. The effects of these 3D features are lost in models that only consider the cells as spheres.<sup>[10]</sup> In addition, the controlled self-assembly of non-spherical particles<sup>[11]</sup> presents expanded possibilities for assembled micromachines.<sup>[12]</sup>

Despite the importance of particle shape, most applications of microparticles still consist of only spherical particles.<sup>[13]</sup> Two dimensional (2D) particle shapes can be produced using a number of techniques, but making non-spherical particles with 3D features in a reproducible and single-step fashion, and with compatible chemistry has remained challenging. Bottom-up bulk emulsification techniques are limited to either spherical or spheroidal shapes, and can only produce monodisperse particles using specially chosen materials.<sup>[14]</sup> Top-down methods, such as femtosecond laser direct writing (FsLDW)<sup>[15]</sup> and multiphoton fabrication<sup>[16,17]</sup> enable highly resolved 3D particles.

However, these approaches are prohibitively time-consuming unit operations. Particle replication in non-wetting templates (PRINT)<sup>[18]</sup> is an alternative multi-step approach for making simple 3D particles, but the range of possible shapes is limited by the mold design.

Microfluidics-based methods for particle synthesis are continuous, and can be multiplexed for higher throughput.<sup>[19]</sup> Spherical and spheroidal particles<sup>[20]</sup> are attainable in droplet-based microfluidic devices where monodisperse precursor droplets are formed in T-junction<sup>[21]</sup> or flow focusing<sup>[22]</sup> geometries, and then polymerized using light or thermal polymerization.

Microfluidic continuous flow lithography (CFL)<sup>[23]</sup> techniques also provide a single-step way to synthesize monodispersed particles, with precise control over desired morphologies, and the ability to utilize a wide variety of biocompatible and functional materials.<sup>[24]</sup> Recently, hydrophobic particles have been made by using parallel flows as lubrication layers in a non-polydimethylsiloxane device. This demonstration potentially broadens the applicability of CFL-based methods.<sup>[25]</sup> An advanced version of CFL is microfluidic stop flow lithography (SFL),<sup>[26]</sup> which has better particle resolution and improved throughput. CFL and SFL are able to produce 2D extruded particles, but controllably synthesizing 3D particles is still difficult with these methods.<sup>[27]</sup> The number of flow-lithography techniques being proposed for the synthesize of 3D particles, namely, stop flow interface lithography,<sup>[28]</sup> lock release lithography,<sup>[29]</sup> soft membrane deformation and optofluidic maskless lithography,<sup>[30]</sup> tuning particle curvature using a tuning fluid,<sup>[31]</sup> and three-dimensional fluidic self-assembly by axis translation of two-dimensionally fabricated microcomponents,<sup>[32]</sup> suggest that a simple flow-lithography method for making complex 3D particles is highly desirable. Yet, all of the existing methods produce particles with limited 3D features, and often require difficult-to-manufacture 3D channels. To date, single-step synthesis of truly 3D particles from a simple 2D microfluidic channel has remained difficult to accomplish.

Here we demonstrate the controlled synthesis of highly curved 3D particles using a variation of the microfluidic SFL method. We exploit the non-uniformity of the photopolymerizing UV light along the light path to create 3D particles inside 2D microchannels. The non-uniformity of UV light intensity and projection shape mainly arises from a combination of the UV absorption by magnetic nanoparticles in the fluid, the radial non-uniformity of polymerizing UV light exposure, the out-of-focus propagation of light, and the discontinuous patterns on our photomasks. While previous microfluidic flow lithography techniques have tried to avoid having non-uniform UV light along the exposure path, in this paper we use opaque magnetic nano-particles in our hydrogel precursor to generate a gradient of the incoming UV light along the channel height,

Mr. N. Hakimi  
MASc candidate, Department of Chemical Engineering  
Ryerson University

135 Kerr Hall South (KHS), 350 Victoria Street  
Toronto, ON, Canada, M5B 2K3

Prof. S. S. H. Tsai  
Department of Mechanical and Industrial Engineering  
Ryerson University  
338B Eric Palin Hall (EPH), 350 Victoria Street, Toronto,  
ON, Canada, M5B 2K3

Prof. C. H. Cheng  
Department of Chemical Engineering  
Ryerson University  
241O Kerr Hall South (KHS), 350 Victoria Street, Toronto  
ON, Canada, M5B 2K3

Prof. D. K. Hwang  
Department of Chemical Engineering  
Ryerson University,  
241K Kerr Hall South (KHS), 350 Victoria Street, Toronto  
ON, Canada, M5B 2K3  
E-mail: dkhwang@ryerson.ca



DOI: 10.1002/adma.201304378

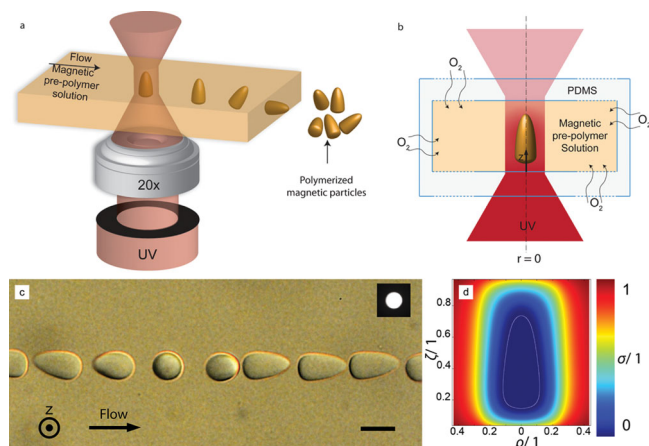


**Figure 1.** Schematic diagram of our particle-synthesis method and experimental images of bullet-shape magnetic microparticles. a) A magnetic precursor solution including monomer, photoinitiator, and hydrophilic ferrofluids flow in the microchannel, and is polymerized by the UV light. Polymerized magnetic particles are manufactured in a conveyor-belt fashion, where the flow stops in fixed time increments and the UV light polymerizes the solution. b) A cross-sectional schematic view of our particle synthesis technique. The UV light gradient in  $z$  direction is primarily produced by opaque nanoparticles in the solution. The amount of polymerization that takes place is controlled by the local UV light intensity and oxygen concentration. The curved shape of the particle results from a combined effect of the UV light gradient and the oxygen concentration gradient. c) A row of freshly formed bullet-shaped magnetic particles synthesized in a 2D 40  $\mu\text{m}$  tall microchannel. Here we use a 20x objective ( $N.A. = 0.4$ ,  $T_{\text{focus}} = 51 \mu\text{m}$ ) to produce a cylindrical UV light path across the channel height. The inset is a picture of the photomask we use. Scale bar 20  $\mu\text{m}$ . d) A numerical simulation of the normalized oxygen concentration and monomer conversion in the cross section of the channel. Due to symmetry we only solve the model for half of the cross section of the polymerization domain. The surface plot represents the oxygen concentration ( $\sigma = [O_2]/[O_{2,\text{req}}]$ ) and the white line represents the critical monomer conversion,  $1 - \xi = 0.02$ , ( $\xi = [M]/[M_0]$ ). The region enclosed by the white contour line has a monomer conversion factor above the threshold level such that the precursor solution solidifies into a gel. Thus, the white contour line also gives a prediction of the particle shape.

to create functional particles with parabolic curvature in a one-step fashion. We also tune the microscope stage height as a control parameter to adjust the shape of the polymerizing UV light. Finally, we combine these two ideas with the use of discontinuous photomask patterns to synthesize 3D particles with elaborate features.

Figure 1a is a schematic diagram of our setup for producing 3D particles. We synthesize hydrogel particles using a stop-flow lithography-based method, where a solution of monomer, photoinitiator, and hydrophilic ferrofluids flow in a microchannel, and is polymerized by projection of a UV light through a photomask. The polydimethylsiloxane (PDMS) microchannels have heights,  $H = 40$  or  $100 \mu\text{m}$ . Experimental images are captured using an SLR camera mounted to our inverted light microscope (See details in Methods section). A row of bullet-shaped curved 3D particles is shown in Figure 1c. These particles are synthesized upstream of the image recording region using a simple 2D circle photomask (inset of Figure 1c), in a PDMS channel with height,  $H = 40 \mu\text{m}$ . The depth of focus of the UV light,

$T_{\text{focus}} = 51 \mu\text{m}$ , and we use a 20x objective with numerical aperture,  $N.A. = 0.4$ . We expect a straight cylindrical UV light path through the thickness of the channel, because the depth of focus is larger than the channel height (see Supporting Information, Section 2). Here, the incoming UV light is not uniform in the radial direction even when the light is focused. After propagating through the photomask hole and the objective lenses, the diffracted light is more intense at the center of its propagation path and its intensity diminishes away from the center. (See Supporting Information, Section 3.)

In most CFL systems, UV absorption by the mixture of monomer and photoinitiator does not produce particles with curved walls.<sup>[23,26,33,35]</sup> This is because the reduction of UV light along the channel height (typically 10–50  $\mu\text{m}$ ) is often negligible (see Supporting Information, Figure S3). In our setup, the inclusion of opaque magnetic nano-particles in the monomer mixture significantly increases the absorptivity of the precursor solution, which affects the penetration of the incident UV radiation by obstructing the UV light. Thus, the UV light intensity substantially diminishes along the channel height. Since the photolysis rate of the initiator, which produces free-radicals, is proportional to the local light intensity, the UV light attenuation leads to a free-radical concentration gradient along the channel height, and in the radial direction. These free-radicals, which can start and carry on the polymerization reactions, are also inhibited by the dissolved oxygen present in the precursor solution. Molecular oxygen prevents the polymerization by reacting with initiator, primary, and polymer radicals to form peroxy radicals.<sup>[34]</sup> Since the peroxy radicals do not facilitate polymerization, the oxygen molecules are essentially scavenging and terminating free radicals. Some of the oxygen consumed in these reactions is replenished by oxygen continually diffusing in through the PDMS walls. This competition between reaction and diffusion of oxygen, ensures that there is an un-cross-linked “lubrication layer” close to the PDMS channel walls.<sup>[35]</sup>

This reaction-diffusion process combined with the non-uniformity (radial and axial) of light intensity produces a gradient of effective free-radical concentration, ranging from a maximum near the bottom center of the channel cross section, to a minimum at the channel walls. As a result, the synthesized magnetic particles have nearly flat bottoms, and curved profiles on the far side of the light source along the channel height (Figure 1c), rather than the symmetric rod shapes typically observed in the absence of absorbing additives.<sup>[23]</sup> At lower parts of the channel height, the incoming UV light produces free-radicals at a sufficiently high rate to offset the effect of oxidation reactions. Thus, in lower regions closer to the UV light source, there are more polymerization reactions, compared to the upper regions of the channel, where the weakened UV light only initiates sufficient polymerization reactions in the inner parts of the light path. In the upper region, precursor close to the center of the light path polymerizes beyond the gelation point, while almost the entire precursor in the lower region of the light path solidifies into a gel. Thus, particles with curved walls are synthesized, and the curvature is enhanced by the radial gradient of the incoming UV light (Supporting Information Figure S2), in the presence of the UV absorbing additive.

We modify the one-dimensional model of Dendukuri *et al.*<sup>[35]</sup> to take into account the two-dimensional diffusion of oxygen as

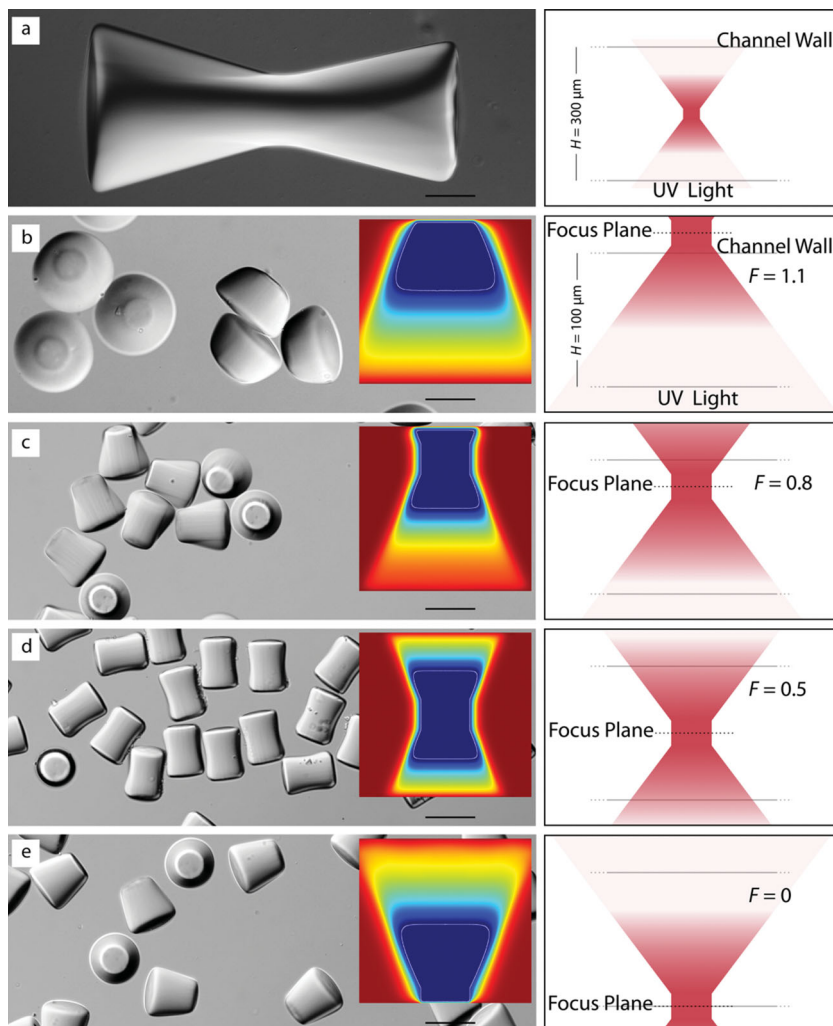


**Figure 2.** Polymeric 3D particles of various shapes, without opaque magnetic material, synthesized using a 40x objective (N. A. = 0.6). a) An hour-glass shaped particle made in a 300  $\mu\text{m}$  tall microchannel, where the UV light is focused at the mid-plane of the channel height ( $F = 0.5$ ). b–e) Highly uniform 3D particles of different shapes made in 100  $\mu\text{m}$  tall microchannels, while changing the objective-to-microchannel distance to obtain different values of relative focal distance,  $F$ . The relative focal distance value,  $F$ , is 0.5, 1.10, 0.80, 0.50 and 0 in a, b, c, d and e, respectively. Scale bars 50  $\mu\text{m}$ . The right panel shows a schematic diagram of focal plane position relative to the channel height in each case. The insets show the simulated oxygen concentration,  $\sigma$ , on a surface plot, and the simulated critical monomer conversion contour,  $1-\xi = 0.02$ , as the white line which gives predicted particle shapes in each case.

well as the radial non-uniformity of the UV light in our setup (see Supporting Information, Section 1). The surface plot in Figure 1d shows the normalized oxygen concentration profile, ( $\sigma = [O_2]/[O_2,eqb]$ ), in the cross section of the channel, where  $[O_2]$  and  $[O_2,eqb]$  are the precursor solution's present and the equilibrium oxygen concentrations, in a PDMS environment, respectively. In Figure 1d, the critical monomer conversion contour  $1-\xi = 0.002$  ( $\xi = [M]/[M_0]$ ), is depicted with the white line.  $[M]$  and  $[M_0]$  are the present and initial monomer concentrations of the precursor solution, respectively. Solidification of the precursor takes place where the monomer conversion is higher than a critical value,  $1-\xi > 0.002$ .<sup>[36]</sup> The region within the white contour shows monomer conversion above the threshold value,

thus giving the predicted particle shape. We use this 2D model to simulate the 3D particle shape because the system is axisymmetric about the  $z$ -axis. The length scales are non-dimensionalized with respect to channel height such that  $\rho = r/H$  and  $\zeta = z/H$ . Having symmetry about the  $z$ -axis also allows us to impose a symmetric boundary condition along the vertical centerline of the polymerization domain, and only solve the model for half of the cross-section domain. We find that our 2D model is able to capture both the curvature and size of the bullet-shaped particles we synthesized in our experiments.

We are also able to synthesize 3D shaped particles in our 2D microfluidic system, without including opaque materials in our precursor solution (Figure 2). We use a high numerical aperture 40x objective (N. A. = 0.60,  $T_{\text{focus}} = 18.5 \mu\text{m}$ ), with  $H = 300 \mu\text{m}$  (to make the hourglass-shaped particle shown in Figure 2a) or 100  $\mu\text{m}$  (to make the particles shown in Figure 2b–e) tall microchannels to achieve a UV light path distinct from the cylindrical light path used previously (Figure 1). The high numerical aperture objective causes the incoming UV light to have higher incident angle, which reduces the depth of focus,  $T_{\text{focus}}$ . This reduction in  $T_{\text{focus}}$ , coupled with microchannels of increased height, results in a polymerization zone that is no longer a vertical cylinder.

Figure 2a shows an hourglass-shaped hydrogel particle polymerized in a 300  $\mu\text{m}$  tall microchannel with a high numerical aperture objective (N. A. = 0.6). Here the objective focus is placed at the mid-plane of the channel height (right schematic diagram of Figure 2a). The synthesized particle is approximately symmetric about its midpoint because the UV absorption of the monomer solution is insignificant. This particle exhibits a structure with two end lobes and a narrow central region, and well represents the shape of the incoming UV light. With this platform, we can use microchannels of a reduced height of 100  $\mu\text{m}$ ,

and simply control the objective-to-microchannel distance to obtain a variety of particle shapes (Figure 2b–e). We define a normalized value for the UV light focal plane position,  $F$ , relative to the bottom of the channel, such that  $F = 1.00$  places the focal plane at the top wall of the channel, and  $F = 0$  corresponds to the UV light focused on the bottom substrate. For example, we can bring the objective close to the microchannel such that  $F = 1.1$ , to obtain a cone-shaped UV light profile (the right schematic of Figure 2b shows this focal plane position). This polymerization zone shape produces particles as seen in Figure 2b. Moving the objective away from the microchannel in a step-wise fashion, such that  $F = 0.80, 0.50$ , and 0, allows us to synthesize particle shapes seen in Figure 2c, 2d, and 2e, respectively.

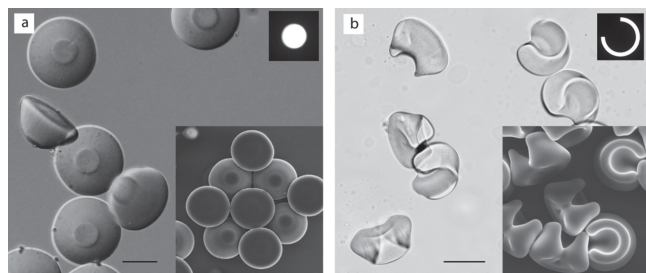


**Figure 3.** Complex-shape magnetic particles synthesized by tuning the UV light focal plane,  $F$ . a) Magnetic particles synthesized by focusing the UV light below the bottom surface of the channel such that  $F = -0.2$ . The bottom right inset shows a SEM image of particles stacked together upon drying. b) Highly curved magnetic particles made by a combination of an alternative photomask pattern (top right inset), the presence of magnetic nanoparticles, and a UV light relative focal distance,  $F = 0$ . Scale bars 50  $\mu\text{m}$ .

A surface plot of the simulated dimensionless oxygen concentration,  $\sigma$ , and the critical monomer conversion contours,  $1-\xi = 0.02$ , of the polymerization region are plotted in the insets of Figure 2b–e. The simulated critical monomer conversion contours (white lines) represent the predicted particle shapes. Here, we extend our numerical model of monomer conversion by capturing the non-cylindrical shape of our UV light paths. The schematic diagrams on the right side of Figure 2 show the normalized UV focal plane position,  $F$ , in each experiment and simulation. We find a good qualitative agreement between the simulated particle shapes and our experimental results, as the simulation is able to capture all of the main features of the synthesized particles, including the particle shape and size.

We can achieve an even higher order of complexity in the morphology of synthesized particles by the combination of tuning of the relative focus plane position  $F$ , and adding opaque magnetic nanoparticles to the precursor solution. This creates a gradient of UV light along the channel height, and a non-cylindrical UV light path. UFO shaped magnetic particles (Figure 3a) are synthesized by applying a simple circle photomask (top right inset of Figure 3a). The UV light is focused to  $F = -0.2$ . A high numerical aperture 40 $\times$  (N. A. = 0.60) objective is used to achieve a cone shaped UV light path along the channel height. Here the local UV intensity is decreased due to the out-of-focus UV light propagation and the presence of opaque magnetic particles. As a result, the precursor solution is only polymerized in a portion of the channel height. The synthesized particles have a UFO shape due to the diverging cone shape of UV light. The bottom right inset of Figure 3a is an SEM image of these UFO shaped particles, after drying, where the particles have stacked into a coherent

pattern that is only possible due to their non-spherical 3D shapes. We can also change the photomask pattern to add to the tunability of our technique. For example, by using an alternate photomask pattern (top right inset of Figure 3b), and setting the focal distance  $F = 0$ , we are able to synthesize 3D particles with high curvature (Figure 3b). The shape of these magnetic particles is controlled by a combination of photomask pattern, magnetic particle concentration, and UV light relative focal plane position,  $F$ .

Exploiting the off-focus UV light propagation using photomasks with disconnected patterns allows for the fabrication of particles with 3D surface features (Figure 4a), asymmetric 3D characteristics (Figure 4b), and branched structures (Figure 4c). The light intensity diminishes as it diverges after passing its focus plane. We use discontinuous photomask patterns, and adjust the pattern spacing, to focus the UV light from a 40 $\times$  objective (N. A. = 0.6), and create different kinds of diverging light paths along the channel height. We find that, if the transparent parts of a discontinuous photomask pattern are close enough to each other, the UV light going through each hole will constructively interfere, and intensify in specific zones. As a result, polymerization does not only occur directly in-line with the photomask pattern. Rather, the monomer solution also polymerizes in zones where UV light constructively interferes. We take advantage of the out-of-focus overlap of UV light through different photomask holes to make single 3D particles, with a range of 3D features.

We have made highly uniform, 3D, magnetic and non-magnetic microparticles using a flow lithography-based method, and in a single-step and controllable fashion. Our particles

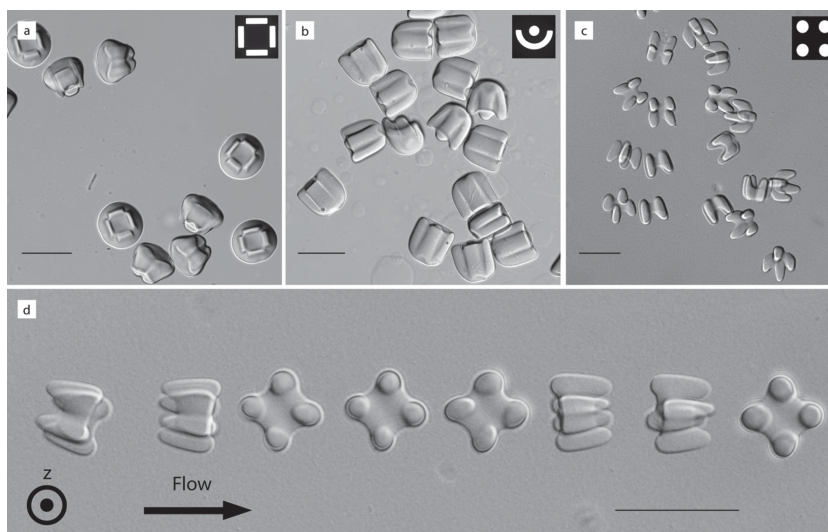


**Figure 4.** A diversity of 3D features, achieved by applying discontinuous photomask patterns, with magnetic precursor solutions, and controlled UV light focal distance  $F$ . a–c) High curvature 3D particles, with 3D surface features (a), asymmetric 3D characteristics (b), and branched structures (c), all synthesized using the method from Figure 3, albeit modified by the use of disconnected patterns on photomasks. The disconnected photomask patterns here cause non-uniform constructive interference of UV light, which allows polymerization of select regions in the polymer solution.  $F$  is  $-0.2$ ,  $0.2$  and  $-0.3$  in a, b and c respectively. d) A succession of newly manufactured particles with branched legs, moving with the fluid flow in a microchannel. The insets of a, b, and c show the photomasks that we use to make the corresponding particles. Scale bars 50  $\mu\text{m}$ .

are based on hydrogel, because hydrogel is used ubiquitously in biotechnology and microfluidics applications. We also add magnetic nanoparticles to the hydrogel, to increase the opacity of the precursor solution, and produce functional magnetic 3D particles. We are convinced that other nanoparticle or monomer solutions, that significantly absorb UV light at this wavelength spectrum, will also produce similar 3D particles using our technique.

The simplicity of our setup makes it possible to couple with other techniques, such as using digital micromirror devices (DMDs) for maskless real-time lithography,<sup>[33]</sup> interface lithography for 3D particles with 3D structures, co-flow formation of Janus particles, and with 3D microchannels to make a wide variety of 3D particles, while maintaining a high throughput that is comparable to that of SFL systems. The technique we introduce may also be capable of controlling the degree of polymerization of different parts of a single particle. The inhomogeneous polymerization of a single particle may result in non-uniform particle responses to environmental stimuli, and particles with inhomogeneous mechanical stability, degradability and elasticity. Finally, since our method is inexpensive and achieves a high production rate, future studies may employ this method to make 3D particles for drug delivery, self-assembly, and other applications that require many particles of controlled 3D shapes. For example, particles with branched 3D structures (Figure 4c) may be used to model atoms and molecules of a complex structure,<sup>[3]</sup> and an array of bullet-shaped particles (Figure 1) may have applications in making micro-needles.

## Experimental Section

**Materials:** The magnetic polymeric microparticles are synthesized from a precursor solution prepared by mixing 35% (v/v) poly(ethylene glycol) (700) diacrylate (PEG-DA 700, Sigma-Aldrich), 5% (v/v) 2-hydroxy-2-methylpropiophenon (Darcour 1173, Sigma-Aldrich) initiator, 20% (v/v) water-based ferrofluid (EMG 508, Ferrotec), and 40% (v/v) water. The non-magnetic particles are prepared using 35% (v/v) PEG-DA 700, 5% (v/v) Darcour 1173, and 60% (v/v) water. Following synthesis, we collected the particles from a reservoir at the downstream of the channel and washed them several times with 0.5% (v/v) Tween-20 (Sigma Aldrich) solution in water.

**Microfluidic Device Fabrication:** We made microfluidic devices by pouring 10:1 (w/w) polydimethyl-siloxane (PDMS, Sylgard 184, Dow Corning) and curing agent on a positive relief patterned silicon wafer (SU-8 photoresist, Microchem) followed by baking at 65 °C for 2 h. After cutting the channels and piercing an inlet and a reservoir, we attached the channels on partially cured (at 65 °C for 25 min) PDMS-coated glass slides. We baked the channels for another 2 h at 65 °C to stably attach the PDMS channel to the glass slides. We assembled pipet tips (ART 10 Reach and ART 200, molecular BioProducts, Inc.) to the inlet of the channel to flow our precursor solutions in the channel. The channels were mounted on an inverted microscope (Axiovert Observer .A1, Zeiss) for particle synthesis.

**Photopolymerization Setup:** We synthesized our particles in a stop-flow lithography based setup. The particles were photopolymerized when the flow is stopped. Then synthesized particles are pushed out of the photopolymerization area by a flow of fresh precursor solution and this cycle repeats. A command script governed a pressure valve (Type 100LR, ControlAir Inc.) to switch between on (allowing a 2 psi air pressure to push the flow in the channel) and off (unpressurized). The script also governed a digital UV shutter (Lambda SC, Sutter Instruments) that was switching between on and off, on the way of UV

illumination from our UV source (Lumen 200, Prior Scientific, Inc.). We used a UV filter (11000v2, Chroma) to select UV light at desired excitation for polymerization. Transparency masks (CAD/Art Services, Inc) were designed with AUTOCAD 2011 and placed at the field-stop of the microscope to shape the UV light. A 20x objective (20x/0.4 korr LD Plan-Neofluar, Zeiss) was used to make a cylindrical UV exposure path throughout the channel height to make the bullet shaped particles (Figure 1a), and a 40x objective (40x/0.6 korr LD Plan-Neofluar, Zeiss) was used to shape the UV light to have a higher incident angle to make particles shown in Figures 2–4. For tuning the focal point of UV light at desired heights of the channel, we first focus the objective at the bottom of the channel so as the clearest image of the glass substrate was achieved. Then the objective-to-stage distance was adjusted by the microscope focus drive to achieve the desired relative focus plane position, knowing that in our microscope, each line of the focus drive represents 2 μm displacement of the microscope stage height. A Nikon D300s camera (DigitalSLR) was used to capture bright field images of the synthesized particles. Finally, we used scanning electron microscopy (FE-SEM S-4500, Hitachi) to capture the images at the bottom left insets of Figure 4.

## Supporting Information

Supporting Information is available from the Wiley Online Library or from the author.

## Acknowledgements

The authors acknowledge comments from Prof. Howard A. Stone and Dr. Janine Nunes. D. K. H. gratefully acknowledges financial support from the Natural Sciences and Engineering Research Council of Canada (NSERC), Discovery grant no. RGPIN/386092–2010.

Received: August 31, 2013

Revised: October 17, 2013

Published online:

- [1] Y. Qiu, K. Park, *Adv. Drug Deliv. Rev.* **2012**, *64*, 49–60.
- [2] B. G. Chung, K. H. Lee, A. Khademhosseini, S. H. Lee, *Lab on a Chip* **2012**, *12*, 45–59.
- [3] S. C. Glotzer, M. J. Solomon, *Nat. Mater.* **2007**, *6*, 557–562.
- [4] S. M. Spearing, *Acta Materialia*. **2000**, *48*, 179–196.
- [5] K. J. Lee, J. Yoon, J. Lahann, *Curr. Opin. Colloid Interface Sci.* **2011**, *16*, 195–202.
- [6] J. A. Champion, Y. K. Katare, S. Mitragotri, *J. Control. Release* **2007**, *121*, 3–9.
- [7] S. Barua, J. W. Yoo, P. Kolhar, A. Wakankar, Y. R. Gokarn, S. Mitragotri, *Proc. Natl. Acad. Sci. USA*. **2013**, *110*, 3270–3275.
- [8] N. Pamme, C. Wilhelm, *Lab on a Chip* **2006**, *6*, 974–980.
- [9] T. Franke, S. Braunmuller, L. Schmid, A. Wixforth, D. A. Weitz, *Lab on a Chip* **2010**, *10*, 789–794.
- [10] S. S. H. Tsai, I. M. Griffiths, H. A. Stone, *Lab on a Chip* **2011**, *11*, 2577–2582.
- [11] S. S. H. Tsai, J. S. Wexler, J. D. Wan, H. A. Stone, *Appl. Phys. Lett.* **2011**, *99*, 153509.
- [12] G. M. Whitesides, B. Grzybowski, *Science* **2002**, *295*, 2418–2421.
- [13] M. Das, H. Zhang, E. Kumacheva, *Ann. Rev. Mater. Res.* **2006**, *36*, 117–142.
- [14] B. R. Saunders, B. Vincent, *Adv. Colloid Interface Sci.* **1999**, *80*, 1–25.
- [15] Y. L. Zhang, Q. D. Chen, H. Xia, H. B. Sun, *Nano Today* **2010**, *5*, 435–448.

- [16] C. N. LaFratta, J. T. Fourkas, T. Baldacchini, R. A. Farrer, *Angew. Chem.-Int. Ed.* **2007**, *46*, 6238–6258.
- [17] S. C. Laza, M. Polo, A. A. R. Neves, R. Cingolani, A. Camposeo, D. Pisignano, *Adv. Mater.* **2012**, *24*, 1304–1308.
- [18] J. P. Rolland, B. W. Maynor, L. E. Euliss, A. E. Exner, G. M. Denison, J. M. DeSimone, *J. Am. Chem. Soc.* **2005**, *127*, 10096–10100.
- [19] T. J. Merkel, K. P. Herlihy, J. Nunes, R. M. Orgel, J. P. Rolland, J. M. DeSimone, *Langmuir* **2010**, *26*, 13086–13096.
- [20] D. K. Hwang, D. Dendukuri, P. S. Doyle, *Lab on a Chip* **2008**, *8*, 1640–1647.
- [21] P. Garstecki, M. J. Fuerstman, H. A. Stone, G. M. Whitesides, *Lab on a Chip* **2006**, *6*, 693–693.
- [22] S. Q. Xu, Z. H. Nie, M. Seo, P. Lewis, E. Kumacheva, H. A. Stone, P. Garstecki, D. B. Weibel, I. Gitlin, G. M. Whitesides, *Angew. Chem.-Int. Ed.* **2005**, *44*, 724–728.
- [23] D. Dendukuri, D. C. Pregibon, J. Collins, T. A. Hatton, P. S. Doyle, *Nat. Mater.* **2006**, *5*, 365–369.
- [24] M. E. Helgeson, S. C. Chapin, P. S. Doyle, *Curr. Opin. Colloid Interface Sci.* **2011**, *16*, 106–117.
- [25] K. W. Bong, J. Xu, J. Kim, S. C. Chapin, M. S. Strano, K. K. Gleason, P. S. Doyle, *Nat. Comm.* **2012**, *3*, 805.
- [26] D. Dendukuri, S. S. Gu, D. C. Pregibon, T. A. Hatton, P. S. Doyle, *Lab on a Chip* **2007**, *7*, 818–828.
- [27] D. Dendukuri, P. S. Doyle, *Adv. Mater.* **2009**, *21*, 4071–4086.
- [28] J. H. Jang, D. Dendukuri, T. A. Hatton, E. L. Thomas, P. S. Doyle, *Angew. Chem.-Int. Ed.* **2007**, *46*, 9027–9031.
- [29] K. W. Bong, D. C. Pregibon, P. S. Doyle, *Lab on a Chip* **2009**, *9*, 863–866.
- [30] S. A. Lee, S. E. Chung, W. Park, S. H. Lee, S. Kwon, *Lab on a Chip* **2009**, *9*, 1670–1675.
- [31] P. Panda, K. P. Yuet, T. A. Hatton, P. S. Doyle, *Langmuir* **2009**, *25*, 5986–5992.
- [32] S. E. Chung, Y. Jung, S. Kwon, *Small* **2011**, *7*, 796–803.
- [33] S. E. Chung, W. Park, H. Park, K. Yu, N. Park, S. Kwon, *Appl. Phys. Lett.* **2007**, *91*, 041106.
- [34] C. Decker, A. D. Jenkins, *Macromolecules* **1985**, *18*, 1241–1244.
- [35] D. Dendukuri, P. Panda, R. Haghgooei, J. M. Kim, T. A. Hatton, P. S. Doyle, *Macromolecules* **2008**, *41*, 8547–8556.
- [36] E. Andrzejewska, *Progress in Polymer Science* **2001**, *26*, 605–665.